Vibrational population transfer between electronic states of N_2^+ in polarization-modulated intense laser fields

Hongqiang Xie,[1,2] Qian Zhang,[1] Guihua Li,[1,3] Xiaowei Wang,[1] Li Wang,[1]
Zhiming Chen,[2] Hongbin Lei,[1] and Zengxiu Zhao[1,*]

[1]*Department of Physics, National University of Defense Technology, Changsha 410073, People's Republic of China*
[2]*State Key Laboratory of Nuclear Resources and Environment, East China University of Technology, Nanchang 330013, People's Republic of China*
[3]*School of Science, East China Jiaotong University, Nanchang 330013, People's Republic of China*

(Received 7 July 2019; published 25 November 2019)

Recently, the significant enhancement of N_2^+ lasing realized with the help of a polarization-gated intense 800-nm pump provides crucial clues to optimize both ionization and population coupling processes occurring during N_2^+ lasing generation [Li *et al.*, Phys. Rev. Lett. **122**, 013202 (2019)]. In this work, we carried out an experimental and theoretical study on the generation of N_2^+ lasing at 391 nm by the use of two different polarization-modulation schemes for pump pulses. It was found that the probe spectra in the vicinity of 391 nm are readily transformed from absorption to lasing due to population depletion of the ground state of N_2^+ just via changing the pump polarization state. More importantly, N_2^+ lasing intensity can be further increased when the pump polarization is modulated with a half-wave plate and a multiple-order quarter-wave plate compared with that obtained by the polarization-gating technique. All the experimental observations are well explained by the different population inversions between the states $B\,^2\Sigma_u^+$ and $X\,^2\Sigma_g^+$ of N_2^+ in polarization-modulated pump laser fields.

DOI: 10.1103/PhysRevA.100.053419

I. INTRODUCTION

Since high-gain air lasing was first discovered during femtosecond laser filaments in past decades, it rapidly received considerable attention because of its promising applications in terms of remote sensing and standoff spectroscopy [1–10]. Particularly, N_2^+ lasing produced via strong field ionization is found to be complicated yet very interesting. Various kinds of molecular quantum coherences including electronic states and rotational coherence could have a significant impact on the generation of N_2^+ lasing [11–16]. The exact amplification mechanism is still under hot debate [17–24], by attributing it to the stimulated emission based on the population inversion between the electronic states of N_2^+ or superradiancelike emission due to the establishment of quantum coherence among molecules. Several groups recently proposed that N_2^+ lasing can be achieved even without population inversion by taking advantage of coherence [25]. One of the major disagreements among those proposals at present is the necessity of the population inversion.

N_2^+ lasing involves the transitions from the second excited electronic state $B\,^2\Sigma_u^+$ (i.e., B) to the ground state $X\,^2\Sigma_g^+$ (i.e., X) of N_2^+. According to Molecular Ammosov-Delone-Krainov (MO-ADK) theory, the population between the states B and X cannot be inverted just by the ionization process alone [26]. It was pointed out theoretically and demonstrated experimentally that the population couplings can take place between the state $X\,^2\Sigma_g^+$ and the intermediate state $A\,^2\prod_u$ (i.e., A) after molecular nitrogen is ionized with 800-nm femtosecond pulses [16,25,27–32]. The population coupling at the falling edge of 800-nm pump pulses could deplete the population of the X state and hence cause the population inversion between the B and X states. In addition, Li and co-workers reported recently that the population inversion can be further enlarged by employing the polarization-gating (PG) technique which is widely applied to generation of isolated attosecond pulses [31,33]. The finding opens a new perspective to optimize both ionization and population coupling processes separately in N_2^+ lasing by shaping the polarization of intense pump pulses.

In this work, we experimentally and theoretically investigate the generation of N_2^+ lasing at 391 nm [$B(v''=0) \rightarrow X(v=0)$] with polarization-modulated intense 800-nm pump pulses. A comparative study on the enhancement of N_2^+ lasing through two different polarization-modulation schemes for the 800-nm pump was conducted. Larger population transfer between $X(v=0)$ and $A(v'=2)$ is achieved experimentally than that obtained with the PG method, leading to a stronger 391-nm lasing. In addition, our results reveal that for 391 nm, the signal could vary from absorption to lasing by properly modulating the polarization of the pump, directly evidencing efficient population transfer from the $X(v=0)$ state to $A(v'=2)$. The combined experimental and theoretical investigations confirm that the population inversion between the states B and X is of significance for N_2^+ lasing to occur at a relatively high gas pressure under our conditions.

*zhaozengxiu@nudt.edu.cn

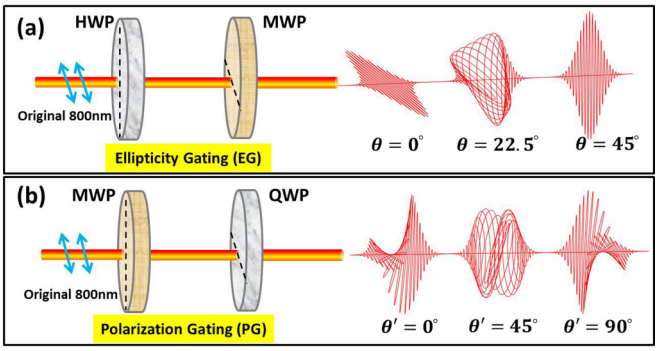

FIG. 1. The intense pump laser polarization modulated with (a) EG (HWP+MWP) scheme, and (b) PG (MWP+QWP) scheme. $\theta(\theta')$ is the angle between the optical axes of HWP and MWP (MWP and QWP).

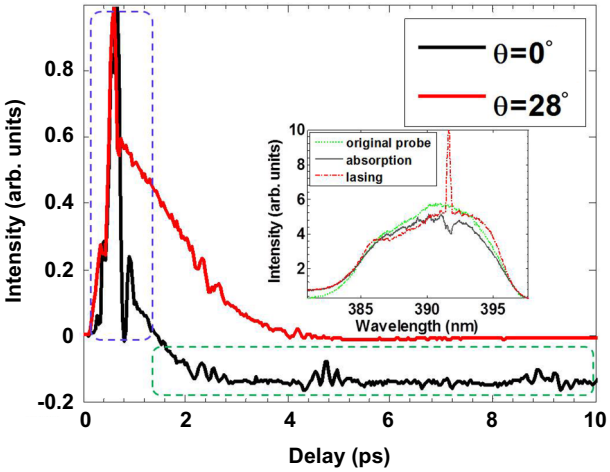

FIG. 2. The normalized spectral intensity at 391 nm (integrated over the wavelength range of 391.1–392 nm) as a function of the time delay between the pump and the probe pulses for $\theta = 0°$ and $\theta = 28°$ with the EG scheme. The inset is a typical absorption and lasing spectrum at the time delay of ~3 ps.

II. EXPERIMENTAL SETUP

The experiments were performed with a commercial Ti:sapphire laser system which delivers femtosecond laser pulses at the center wavelength ~800 nm, with the pulse energy ~4 mJ, pulse width ~35 fs, and repetition rate 1 kHz. The output 800-nm laser pulses were split into two parts with a 70%:30% beam splitter. The main pulse with the energy of ~1.95 mJ served as the pump. The other beam, after being frequency doubled by a 0.2-mm-thick β-barium borate crystal, was used as the probe. A Glan-Taylor prism was put in the probe-beam path to ensure that the probe pulse was strictly linearly polarized. The polarization direction of the pump without modulation was kept the same as that of the probe.

We exploited two different modulation schemes for tuning the pump polarization, as shown in Figs. 1(a) and 1(b). In Fig. 1(a), one half-wave plate (HWP) and one multiple-order quarter-wave plate (MWP, the order $n = 11$) were inserted into the pump beam. We refer to this modulation scheme as ellipticity gating (EG) in the following. The optical fast axis of the MWP was fixed parallel to the original 800-nm pump and θ represents the angle between the optical fast axes of the two plates. The 800-nm pump pulse after passing through MWP is separated into an ordinary light (o light) and an extraordinary light (e light). The e light lags behind the o light by ~29 fs in the time domain. Both e light and o light can produce ionization and couplings, which are determined by their peak intensities. By rotating the optical axis of the HWP, the relative intensity of o light and e light is varied. The resulting polarization after passing through MWP in general varies with time. In the central part of the laser pulse, the electric field is elliptically polarized because of time overlapping of ordinary light (o light) and extraordinary light (e light), while the front and the rear parts correspond to o light and e light, respectively, whose electric fields are linearly polarized and mutually perpendicular. The polarization states of the pump for $\theta = 0°$, $\theta = 22.5°$, and $\theta = 45°$ are also shown in Fig. 1(a). The second modulation method is shown in Fig. 1(b), which is the so-called polarization-gating (PG) technique [31,33,34]. One MWP and a zero-order broad-band quarter-wave plate (QWP) were placed in the pump beam. The optical fast axis of MWP in this case was set to be 45° with respect to the original 800-nm pump polarization direction and θ' represents the angle between the optical fast axes of the MWP and the QWP. The polarization states of the pump for $\theta' = 0$, $\theta' = 45°$, and $\theta' = 90°$ are shown in Fig. 1(b).

The time delay between the polarization-modulated pump and the probe pulse was controlled by a motorized translation stage with a resolution of ~670 as. The pump and probe pulses were combined with a dichromatic mirror (high reflectivity at ~800 nm and high transmission at ~400 nm), and then were focused with an $f = 30$ cm lens into a gas chamber filled with nitrogen at the pressure of 100 mbar. The focused peak intensities of the pump laser without polarization modulation supposing a linear propagation can reach a maximum of $\sim 7 \times 10^{15}$ W/cm^2. The generated forward lasing signals after being collimated by an $f = 25$ cm lens were collected with a grating spectrometer (Kymera-328I, Andor). Lastly, in the measurement of a weak fluorescence signal when needed, we blocked the probe pulse to avoid population depletion of state B by seed amplification process. The backward fluorescence was separated with a dichromatic mirror (high transmission at ~800 nm and high reflectivity at ~400 nm) and then was collected by an $f = 5$ cm lens and was guided into a grating spectrometer via a $2f$-$2f$ imaging scheme. The fluorescence signal was obtained by the accumulation over 1000 laser shots.

III. RESULTS AND DISCUSSION

In the EG scheme, the pump polarization was modulated with a HWP and a MWP, as shown in Fig. 1(a). The normalized N_2^+ lasing intensity at 391 nm (integrated over the wavelength range of 391.1–392 nm) as a function of the pump-probe delay for $\theta = 0°$ is shown in Fig. 2. Positive and negative values of the longitudinal coordinates mean lasing and absorption, respectively. Interestingly, at this gas pressure (i.e., 100 mbar), it can be clearly seen from the black solid

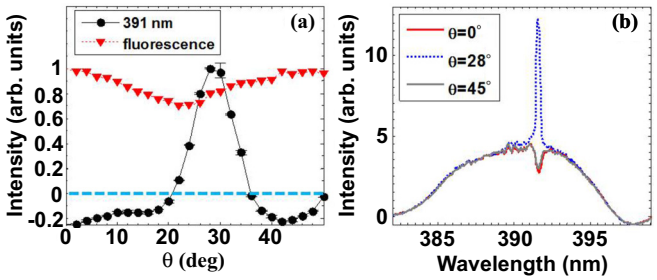

FIG. 3. (a) The normalized spectral intensity at 391 nm (integrated over the wavelength range of 391.1–392 nm) and backward fluorescence signals as a function of θ with the EG modulation scheme. (b) The seed spectrum at $\theta = 0°$, $\theta = 28°$, and $\theta = 45°$.

curve that the weak probe pulse was amplified when the delay was less than ∼1.5 ps, while the absorption dominates when the delay was larger than that. Typical lasing and absorption spectra at the pump-probe delay ∼3 ps are given as an inset in Fig. 2. For comparison, the delay-dependent 391-nm lasing for the optimized θ which is about 28° under our experimental conditions was also depicted by a red solid curve in Fig. 2. Apparently, the time duration for lasing is prolonged to ∼4 ps with the polarization-modulated pump in the latter case.

Next, we examined the 391-nm lasing intensity and backward fluorescence as a function of θ at the time delay of ∼3.2 ps, avoiding delays of molecular alignment. The results are presented in Fig. 3. It can be seen from Fig. 3(a) that the probe pulse was absorbed when θ ranges from 0° to 20°, and subsequently lasing starts to appear and reaches the maximum intensity at $\theta = 28°$; then the lasing signal rapidly decreases with increasing θ until the absorption again appears at $\theta = 36°$. For backward fluorescence, the 391-nm signal first shows a gradual decay until the minimum is obtained at $\theta = 22°$, and the maximum value is reached at $\theta = 0°$ or $\theta = 45°$, i.e., linear polarization. It should be noted that at $\theta = 22°$, the peak intensity of the pump is the lowest because the ordinary light and extraordinary light after transmitting through the MWP share the same intensity. Since fluorescence intensity only reflects the population on the upper state (i.e., B), the population on state B at $\theta = 22°$ is reduced by 30% compared to that prepared with linearly polarized pump pulses. Figure 3(b) shows the lasing spectrum for $\theta = 28°$, and the absorption spectra for $\theta = 0°$ and $\theta = 45°$. The absorption is larger at $\theta = 0°$ than that at $\theta = 45°$ because the interaction of the pump and the probe pulses is stronger for the parallel case (i.e., $\theta = 0°$) than the perpendicular case (i.e., $\theta = 45°$). The experimental results clearly showed the transition from absorption to lasing by modulating the pump polarization. The lasing yields at $\theta = 28°$ are highest while the population of the B state remains relatively small. The observation indicates that there exists efficient vibrational population transfer between $X(v = 0)$ and $A(v' = 2)$ via resonant coupling by the pump pulse as shown below.

It is well known that the stimulated emission based on population inversion depends on the population of not only the upper level (i.e., B) but also the lower level (i.e., X), which is determined by tunnel ionization and population couplings. Since population coupling corresponds to one-photon vertical transition between the states X and A of N_2^+ at 800 nm, the maximum population inversion can be achieved by simultaneously optimizing ionization and coupling processes. It should be noted that the 391-nm lasing intensity can be very strong for the angles of $\theta = 24°$–$34°$ even though the populations of the upper level $B(v'' = 0)$ are reduced comparing with that obtained by a linearly polarized pump, i.e., $\theta = 0°$ or $\theta = 45°$, which implies that population reduction of the lower level $X(v = 0)$ caused by resonant coupling between $X(v = 0)$ and $A(v' = 2)$ should be much larger than that because of ionization. It is worth mentioning that the gas pressure has a great impact on the 391-nm lasing intensity. At a low pumping intensity, lasing can only be generated at a gas pressure below 30 mbar [35]. If the gas pressure is improved to ∼100 mbar, a higher pumping intensity is needed to create 391-nm N_2^+ lasing, as indicated in Ref. [6]. We chose the gas pressure at 100 mbar, which permits us to observe apparent transition from absorption to stimulated emission with polarization-modulated laser fields.

In the second scheme, the pump polarization was modulated with the polarization-gating method which is similar to that used in the reported work [31], as shown in Fig. 1(b). In this measurement, the time delay between the pump and probe was kept at 1.8 ps. Figure 4(a) shows the measured lasing intensities of 391 nm as a function of θ' by rotating the QWP. The backward fluorescence was also recorded for examining the population of the upper level B, which is roughly a constant for variable θ' in this case. The simultaneous measurements of 391-nm lasing and the backward fluorescence signifies that the population of the lower level X of N_2^+ is modulated by controlling the polarization of the pump.

The detailed spectra for 391 nm at several special θ' are depicted in Fig. 4(b). It is worth mentioning that when the optical axes of both the MWP and QWP are adjusted to be parallel to the original 800-nm polarization direction, the incident laser polarization remains unchanged, i.e., linear polarization (LP). For 391 nm, it can be clearly seen that the probe spectrum is absorbed if the incident pump polarization is linear, whereas it becomes amplified with the PG method. It should be also pointed out that the measured dependence of the 391-nm lasing signal on $\theta'$is slightly different from that in the prior work [31]. The deviations may originate from the different MWP and the gas pressure in our experiments. The order of multiple quarter-wave plate we employed is $n = 11$, which is $n = 7$ in the prior work [31]. For an ultrashort femtosecond laser pulse (∼35 fs) with a broadband spectrum, the MWP is not strictly a quarter-wave plate. Hence, in our case, the polarization of the pump laser pulses may not be precisely symmetric about $\theta' = 0°$ because of dispersion introduced by the MWP. Furthermore, the gas pressure could influence the N_2^+ gain behaviors, thereby providing a possibility to show some impact on the asymmetric dependence of lasing signal on the inter-wave-plate angle. Note that there exists another mechanism of lasing based on the electronic, vibrational, and rotational coherence [16,25,32] which can be significantly affected by the gas pressure and the polarization states of the pumping and seeding light.

Lastly, we compare the maximum 391-nm lasing intensity achieved with the two modulation schemes at the optimum

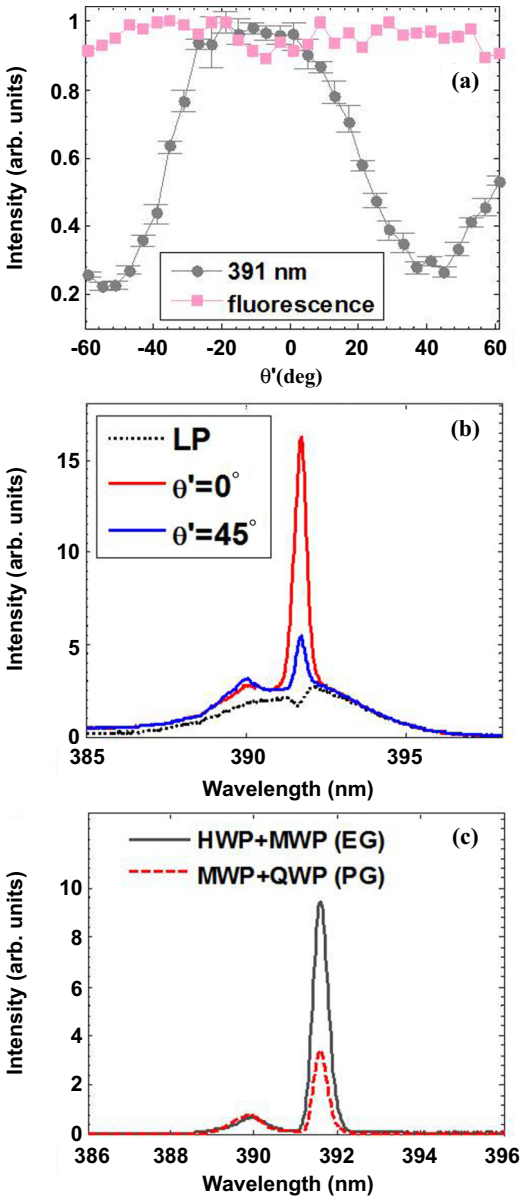

FIG. 4. (a) The normalized spectral intensity at 391 nm (integrated over the wavelength range of 391.1–392 nm) and backward fluorescence signals as a function of θ' with PG modulation scheme. (b) The lasing spectra at $\theta' = 0^\circ$, $\theta' = 45^\circ$ and the absorption spectrum under the linearly polarized (LP) pump. (c) The maximum lasing intensity comparison with the EG modulation scheme and PG modulation scheme.

angles for $\theta \approx 28^\circ$ and $\theta' \approx -10^\circ$, respectively. To ensure the same experimental condition, the probe pulse was blocked to avoid the difference of the pump-probe delay introduced by the used wave plates. We roughly estimated the focused peak intensities by supposing a linear propagation; they are 5×10^{15} and 4.5×10^{15} W/cm^2 for the EG and PG schemes. As shown in Fig. 4(c), the 391-nm lasing signal generated with the EG method is ~2 times stronger than that with the PG scheme, which implies that N_2^+ lasing can be further enhanced by optimizing ultrafast ionization and subsequent population coupling, respectively. A better modulation scheme for

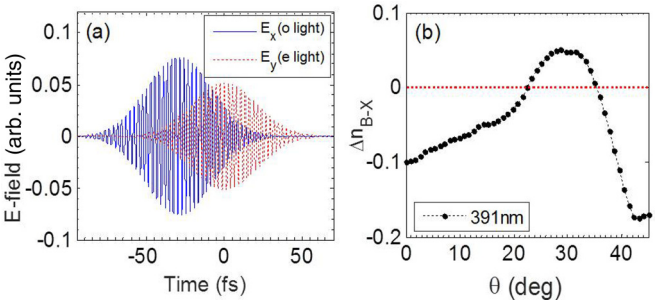

FIG. 5. (a) Time profiles of the electric fields of o light and e light for $\theta = 28^\circ$ with the EG scheme. (b) The calculated population inversion Δn_{B-X} between states B and X as a function of θ.

800-nm pump polarization to enhance N_2^+ lasing in air is in progress.

To quantitatively demonstrate the efficient population transfer by the pump laser fields whose polarizations are modulated with the above-mentioned two schemes, we numerically solved time-dependent three-channel coupled Schrödinger equations,

$$i\hbar\frac{\partial}{\partial t}\begin{pmatrix}\Psi_X(R,t)\\ \Psi_A(R,t)\\ \Psi_B(R,t)\end{pmatrix} = \begin{pmatrix} V_X & E(t)D_{XA} & E(t)D_{XB}\\ E(t)D_{XA} & V_A & 0\\ E(t)D_{XB} & 0 & V_B\end{pmatrix} \times \begin{pmatrix}\Psi_X(R,t)\\ \Psi_A(R,t)\\ \Psi_B(R,t)\end{pmatrix}, \quad (1)$$

where $\Psi_X(R,t)$, $\Psi_A(R,t)$, and $\Psi_B(R,t)$ are, respectively, the wave functions of the three involved electronic states (i.e., X, A, and B) of N_2^+ in the coupling model. For each electronic state, we solely take vibrational states into account while neglecting molecular rotation. The matrix V_X, V_A, and V_B represents the potential energy curves. $E(t)$ is the polarization-modulated pump laser field. D_{XA} and D_{XB} are the dipole transition matrix elements between the corresponding electronic states. It is worth noting that the dipole transition between states X and A is perpendicular to the molecular axis whereas the dipole transition between states X and B is parallel to the molecular axis. One-photon transition is forbidden between states A and B because of symmetry.

In the EG case, the time profiles of o light and e light for $\theta = 28^\circ$ are plotted in Fig. 5(a). Molecular ionization is more efficient when the molecules are aligned along the polarization direction of the pump laser field whereas population coupling requires the molecular axis to be vertical to the polarization direction of the pump laser field. This means when o light is used to ionize nitrogen molecules, e light plays a decisive role in population coupling and vice versa. Therefore, the total population inversion at different θ between states B and X can be reasonably given by

$$\Delta n_{B-X}(\theta) = w_o(\theta)\Delta n^e_{B-X}(\theta) + w_e(\theta)\Delta n^o_{B-X}(\theta), \quad (2)$$

where $w_o(\theta)$, and $w_e(\theta)$ denote the respective ionization caused by o light and e light at different θ. $w_o(\theta)$, and $w_e(\theta)$ are calculated with MO-ADK theory [26]. $\Delta n^e_{B-X}(\theta)$ is the generated population difference due to the coupling between

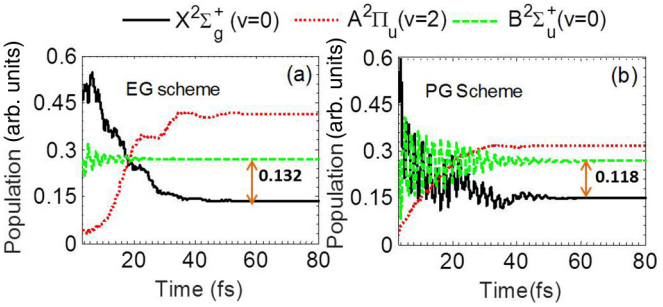

FIG. 6. The population evolution of three electronic states X, A, and B of N_2^+ in a pump laser field whose polarization is modulated by (a) the EG scheme and (b) the PG scheme.

states X and A by e light after ionization by o light. Likewise, $\Delta n^o_{B-X}(\theta)$ is the achieved population inversion by o light after ionization by e light. Both the population differences will be derived from the numerical simulation during the post-ionization propagation of the three-state coupled Schrödinger equation.

In the numerical simulation, the peak pump laser intensity considering the effect of intensity clamping is estimated to be $I = 1.4 \times 10^{14}\,W/\mathrm{cm}^2$, the pulse duration $\tau = 35$ fs, and the center wavelength $\lambda = 800$ nm. The population ratio of electronic states X, A, and B after ionization is assumed to be 0.5, 0.2, and 0.3. We chose these populations based on calculations that are the subject of other work that has been submitted for publication [36]. Since the N_2^+ fluorescence varies with θ, the population of electronic states X, A, and B at various θ is approximately given by $0.5I_f(\theta)$, $0.2I_f(\theta)$, and $0.3I_f(\theta)$. $I_f(\theta)$ is the measured 391-nm fluorescence intensity at θ. Besides, we assume after the generation of N_2^+, the remainder of the pulse is involved in the multiple state coupling. Moreover, considering molecular anisotropic distribution caused by ionization, we calculated the population inversion when the molecular axis is aligned to be 0°, 30°, 60°, and 90° with respect to the polarization direction of the ionization pulse. The final population inversion Δn_{B-X} is obtained after a weighted average according to their ionization probability.

Figure 5(b) shows the calculated population difference Δn_{B-X} between the states B and X as a function of θ. It can be seen that the population difference Δn_{B-X} is above zero over the range of $\theta = 20$–$35°$ and is a negative for all the other θ, which agrees well with the experimental observations in Fig. 3(a) that the stimulated absorption occurs when the population inversion is not achieved and lasing appears only under the condition of $\Delta n_{B-X}(\theta) > 0$. The maximum population inversion Δn_{B-X} is reached at $\theta = 28°$, giving rise to the strongest lasing creation. Therefore, we conclude that the realization of population inversion plays a decisive role for the generation of N_2^+ air lasing at a high gas pressure.

Figures 6(a) and 6(b) show the population evolution of the three electronic states X, A, and B in the pump laser field with polarization modulated by the EG scheme and the PG scheme, respectively. θ and θ' are set to be at the optimum angles. The molecular axis is aligned parallel to the polarization of the ionization pulse. It can be seen for both cases that the population transfer from $X(v = 0)$ to $A(v' = 2)$ starts to emerge after ionization owing to resonant coupling. However, the coupling efficiency by the EG scheme is higher than that by the PG scheme, resulting in a larger population inversion $\Delta n_{B-X} \sim 0.132$ with the EG than $\Delta n_{B-X} \sim 0.118$ achieved with PG at the end of the pump pulse. This qualitatively explains that the measured N_2^+ lasing intensity is much stronger with the EG scheme than with the PG scheme. It should be noted that in the current model the efficiency of population transfer from the X state to the A state depends on the respective contributions to ionization and coupling by the o light and e light. Therefore, the assumption of the relative populations in the three ionic states does not affect the conclusion that the transfer efficiency with the EG scheme is higher than that with the PG scheme qualitatively. The possible physical mechanism behind this is that for the HWP+MWP modulation scheme, o light polarization is always perpendicular to the e light polarization, which is more favorable to balance the ionization and coupling process than that using a time-varying linearly polarized laser field (i.e., PG, $\theta' = 0°$). In fact, the delay between o light and e light can be further optimized by changing the thickness of the MWP to reap a greater population inversion.

To conclude, we directly demonstrated the population transfer between the electronic states $A\,^2\prod_u$ and $X\,^2\Sigma_g^+$ by observing the transformation of absorption and lasing at 391 nm in a pump laser field with polarization shaped by ellipticity gating. Previous investigations show that at the gas pressure of 100 mbar, only absorption appears for a linearly polarized laser pulse with low pumping intensity. However, N_2^+ lasing can be created when using a polarization-state-modulated pump, which can effectively control the coupling strength between the electronic states $A\,^2\prod_u$ and $X\,^2\Sigma_g^+$. It was also revealed that by our proposed ellipticity gating scheme herein, N_2^+ lasing intensity can be further enhanced than that achieved by the reported PG modulation scheme. Such improvement of the N_2^+ lasing signal can be of great use in remote sensing where gas pressure is too high to allow the generation of intense N_2^+ lasing.

ACKNOWLEDGMENTS

This work is supported by the Major Research plan of NSF (Grant No. 91850201), the National Natural Science Foundation of China (Grants No. 61705034, No. 61605227, and No. 11704066), the Natural Science Foundation of Jiangxi Province (Grant No. 20171BAB211007), and the Science and Technology Project of Jiangxi Provincial Education Department (Grants No. GJJ160587 and No. GJJ160576).

H.X. and Q.Z. contributed equally to this work.

[1] Q. Luo, W. Liu, and S. L. Chin, Appl. Phys. B **76**, 337 (2003).

[2] J. Yao, B. Zeng, H. Xu, G. Li, W. Chu, J. Ni, H. Zhang, S. L. Chin, Y. Cheng, and Z. Xu, Phys. Rev. A **84**, 051802(R) (2011).

[3] A. Dogariu, J. B. Michael, M. O. Scully, and R. B. Miles, Science **331**, 442 (2011).

[4] D. Kartashov, S. Ališuskas, G. Andriukaitis, A. Pugžlys, M. Shneider, A. Zheltikov, S. L. Chin, and A. Baltuška, Phys. Rev. A **86**, 033831 (2012).

[5] A. J. Traverso, R. Sanchez-Gonzalez, L. Yuan, K. Wang, D. V. Voronine, A. M. Zheltikov, Y. Rostovtsev, V. A. Sautenkov, A. V. Sokolov, S. W. North, and M. O. Scully, Proc. Natl. Acad. Sci. USA **109**, 15185 (2012).

[6] Y. Liu, Y. Brelet, G. Point, A. Houard, and A. Mysyrowicz, Opt. Express. **21**, 22791 (2013).

[7] J. Yao, G. Li, C. Jing, B. Zeng, W. Chu, J. Ni, H. Zhang, H. Xie, C. Zhang, H. Li, H. Xu, S. L. Chin, Y. Cheng, and Z. Xu, New J. Phys. **15**, 023046 (2013).

[8] J. Yao, G. Li, X. Jia, X. Hao, B. Zeng, C. Jing, W. Chu, J. Ni, H. Zhang, H. Xie, C. Zhang, Z. Zhao, J. Chen, X. Liu, Y. Cheng, and Z. Xu, Phys. Rev. Lett. **111**, 133001 (2013).

[9] S. Mitryukovskiy, Y. Liu, P. Ding, A. Houard, and A. Mysyrowicz, Opt. Express **22**, 12750 (2014).

[10] H. Xie, G. Li, W. Chu, B. Zeng, J. Yao, C. Jing, Z. Li, and Y. Cheng, New J. Phys. **17**, 073009 (2015).

[11] L. Arissian, B. Kamer, A. Rastegari, D. M. Villeneuve, and J. C. Diels, Phys. Rev. A **98**, 053438 (2018).

[12] H. Zhang, C. Jing, J. Yao, G. Li, B. Zeng, W. Chu, J. Ni, H. Xie, H. Xu, S. L. Chin, K. Yamanouchi, Y. Cheng, and Z. Xu, Phys. Rev. X **3**, 041009 (2013).

[13] H. Xie, B. Zeng, G. Li, W. Chu, H. Zhang, C. Jing, J. Yao, J. Ni, Z. Wang, Z. Li, and Y. Cheng, Phys. Rev. A **90**, 042504 (2014).

[14] A. Azarm, P. Corkum, and P. Polynkin, Phys. Rev. A **96**, 051401(R) (2017).

[15] Z. Liu, J. Yao, J. Chen, B. Xu, W. Chu, and Y. Cheng, Phys. Rev. Lett. **120**, 083205 (2018).

[16] J. Chen, J. Yao, H. Zhang, Z. Liu, B. Xu, W. Chu, L. Qiao, Z. Wang, J. Fatome, O. Faucher, C. Wu, and Y. Cheng, Phys. Rev. A **100**, 031402(R) (2019).

[17] G. Li, C. Jing, B. Zeng, H. Xie, J. Yao, W. Chu, J. Ni, H. Zhang, H. Xu, Y. Cheng, and Z. Xu, Phys. Rev. A **89**, 033833 (2014).

[18] Y. Liu, P. Ding, N. Ibrakovic, S. Bengtsson, S. Chen, R. Danylo, E. R. Simpson, E. W. Larsen, X. Zhang, Z. Fan, A. Houard, J. Mauritsson, A. L'Huillier, C. L. Arnold, S. Zhuang, V. Tikhonchuk, and A. Mysyrowicz, Phys. Rev. Lett. **119**, 203205 (2017).

[19] A. Zhang, Q. Q. Liang, M. W. Lei, L. Q. Yuan, Y. Liu, Z. Q. Fan, X. Zhang, S. L. Zhuang, C. Y. Wu, Q. H. Gong, and H. B. Jiang, Opt. Express **27**, 12638 (2019).

[20] M. Britton, P. Laferriere, D. H. Ko, Z. Li, F. Kong, G. Brown, A. Naumov, C. Zhang, L. Arissian, and P. B. Corkum, Phys. Rev. Lett. **120**, 133208 (2018).

[21] B. Zeng, W. Chu, G. Li, J. Yao, H. Zhang, J. Ni, C. Jing, H. Xie, and Y. Cheng, Phys. Rev. A **89**, 042508 (2014).

[22] Y. Liu, P. Ding, G. Lambert, A. Houard, V. Tikhonchuk, and A. Mysyrowicz, Phys. Rev. Lett. **115**, 133203 (2015).

[23] G. Li, H. Xie, Ziting Li, J. Yao, W. Chu, and Y. Cheng, High Power Laser Sci. Eng. **5**, e26 (2017).

[24] B. Xu, J. Yao, Y. Wan, J. Chen, Z. Liu, F. Zhang, W. Chu, and Y. Cheng, Opt. Express **27**, 18262 (2019).

[25] A. Mysyrowicz, R. Danylo, A. Houard, V. Tikhonchuk, X. Zhang, Z. Fan, Q. Liang, S. Zhuang, L. Yuan, and Y. Liu, APL Photon. **4**, 110807 (2019).

[26] X. M. Tong, Z. X. Zhao, and C. D. Lin, Phys. Rev. A **66**, 033402 (2002).

[27] J. Yao, S. Jiang, W. Chu, B. Zeng, C. Wu, R. Lu, Z. Li, H. Xie, G. Li, C. Yu, Z. Wang, H. Jiang, Q. Gong, and Y. Cheng, Phys. Rev. Lett. **116**, 143007 (2016).

[28] H. Xu, E. Lötstedt, A. Iwasaki, and K. Yamanouchi, Nat. Commun. **6**, 8347 (2015).

[29] H. L. Xu, E. Lötstedt, T. Ando, A. Iwasaki, and K. Yamanouchi, Phys. Rev. A **96**, 041401(R) (2017).

[30] Y. Y. Zhang, E. Lötstedt, and K. Yamanouchi, J. Phys. B: At., Mol. Opt. Phys. **52**, 055401 (2019).

[31] H. L. Li, M. Y. Hou, H.W. Zang, Y. Fu, E. Lötstedt, T. Ando, A. Iwasaki, K. Yamanouchi, and H. L. Xu, Phys. Rev. Lett. **122**, 013202 (2019).

[32] A. Zhang, M. Lei, J. Gao, C. Wu, Q. Gong, and H. Jiang, Opt. Express **27**, 14922 (2019).

[33] M. Chini, K. Zhao, and Z. H. Chang, Nat. Photonics **8**, 178 (2014).

[34] B. Shan, S. Ghimire, and Z. H. Chang, J. Mod. Opt. **52**, 277 (2004).

[35] X. Zhong, Z. Miao, L. Zhang, H. Jiang, Y. Liu, Q. Gong, and C. Wu, Phys. Rev. A **97**, 033409 (2018).

[36] Q. Zhang, H. Xie, G. Li, W. Xiao, H. Lei, J. Zhao, Z. Chen, J. Yao, Y. Cheng, and Z. Zhao, arXiv:1911.01563v1.